Exploring altitudinal resolution of Twilight airglow red lines using Twilight Photometer

Pratibha B. Mane

Fergusson College, Pune-411 004, Maharashtra state, India

Corresponding author: pratibhabm263@gmail.com

Keywords: Twilight airglow, Twilight Photometer, Atmospheric aerosols, Remote sensing

Abstract

Twilight Photometer observations were carried out at low latitude station Kolhapur ($16^0$39'42.2" N, $74^0$14'20.8" E) India, during the period 1 January 2009 to 31 December 2011 to yield a reasonable qualitative picture of the day-to-day variability of the vertical distribution of the atmospheric aerosols from about 6 km to a maximum of 350 km. In this study an attempt was made to observe twilight airglow red lines using the vertical profiles of aerosols. The rate of change of red light due to the twilight airglow shows narrow peaks with ~ 600-1000% rise in intensity than due to aerosol twilight glow. The principal aspiration of this study is to highlight the conspicuous capability of Semiautomatic twilight photometer to study the twilight airglow emission lines. Twilight Photometer, although currently seldom used, is still a very effective and the most appropriate ground based passive remote sensing tool for long-term monitoring of different atmospheric components in a wide range of altitude for day-to-day basis. It is an efficient system having a simple and inexpensive underlying principle of operations, yet exhibits extremely accurate and precise usage and can be operated by even a person of average skill. However, it can be seen that the resultant data was consistent with nearest peer technologies, such as LIDARs, Balloon-Borne instruments, rocket measurements, satellite observations etc. It is the first attempt in India to obtain the twilight airglow data using Twilight photometer.

1. INTRODUCTION

Twilight sounding method (TSM) is widely used by several investigators in all over the world to study the atmospheric aerosols (microscopic suspended particles of dust, soot, smoke, or chemicals) (Jadhav et al. 2000). The observations of the rate of change of zenith sky illumination during the twilight period were carried out at low latitude station Kolhapur ($16^0$39'42.2" N, $74^0$14'20.8" E), during the period 1 January 2009 to 31 December 2011, using newly developed Semiautomatic Twilight Photometer. In this study an attempt was made to observe twilight airglow red lines.

The airglow is the radiation emitted over a wide spectrum originating from the chemical de-excitation of molecules in the mesosphere and thermosphere (Bellisario et al. 2020). Discovered by Meinel (1950), it has been studied for decades. First investigations were made by ground-based observations (Chamberlain & Roesler, 1955) and rocket measurements (Baker & Stair, 1988). Satellites allowed direct observation of the nightglow outside the atmosphere with a large spatial and temporal coverage. Among them, HRDI (Burrage et al., 1994), SABER (Marsh et al., 2006), WINDII (Shepherd et al., 2012), or more recently GOMOS (Bellisario et al., 2014) built the main climatology of the various sources of the nightglow.

The airglow i.e. photochemical luminescence (which is also called chemiluminescence) is caused by the chemical reactions of incoming solar radiation with atoms and molecules present in the upper atmosphere. Sunlight supplies the energy needed to raise these materials to excited states, and these excited atmospheric molecules and atoms return to their ground state producing emissions at particular wavelengths (Rafferty, 2015). The airglow is accordingly very broadly classified as day-airglow, twilight airglow, and night airglow (Chattopadhyay & Midya, 2006). The twilight glow is defined as the airglow emission at a time when sunlight is shining on the emitting region of the atmosphere from below. This is distinct from the dayglow where the sunlight enters from above, and from the nightglow where sunlight is absent. The definition implies that the sunlight is responsible for the excitation of the twilight glow in a direct or indirect manner (Agashe 1987). The twilight airglow is further classified as: Morning twilight airglow and Evening twilight airglow. Among the various sources of emission, the Airglow contributions average 40 percentages of total brightness of the sky that can be observed in a moonless night.

The Twilight photometric data provides vital statistical information about attitudinal separation of Twilight airglow red lines. As soon as the sun has just set, the brightness of the sky decreases rapidly, thereby enabling us to see the airglow that is caused from such high altitudes that they are still fully sunlit until the sun drops more than about 18° below the horizon. During this time, red emissions from the sodium layer and 630 nm oxygen lines are dominant, during civil and nautical twilight. Once astronomical darkness has set in, the emission line due to formation of Nitric oxide is dominant, and atmospheric scattering of starlight occurs.

The twilight sounding method (TSM), although they have a much longer observational history in the field of atmospheric aerosols, can be used for Twilight glow observations. Here, the earth's shadow scans through the emission layer giving valuable altitudinal information; at the same time, it leaves the lower atmosphere in the dark and facilitates observations. Hunten (1967) made the interpretation of twilight measurements by using Spectrographs are identical with those designed for aurora and nightglow studies having very high speed. Swider (1969) has suggested that Simultaneous measurements of several spectral emissions during twilight would be useful and would help to define the energy range of the electrons involved. Thus, a measurement at the time when there is topside excitation, that is, when the conjugate point is sunlit, should give a different and higher profile than either the day glow or nightglow.

Researchers all over the world used various instruments to sturdy twilight airglow phenomenon. Pick et al. (1971) conducted twilight airglow measurements of OH and O_2 using Balloon-Borne instruments. A gondola carrying a grating spectrometer for the 1–2 μ region and filter photometers with pass bands at 1.27 μ and 1.66 μ was flown from Fort Churchill. The equipment was maintained at a height of 42 km through evening and morning twilights. The variation of the O_2 IR atmospheric band at 1.27 μ was measured for morning and evening high latitude summer twilight. Moreels et al. (1973) designed and constructed the high-altitude Balloon-borne three-channel day glow photometer with the intention of making a series of observations of the Q branch of the OH 8-6 band during flights through morning and evening twilights. Moos & Fastie (1967) reported far UV photometer measurements of the (dawn) twilight airglow. Optical emissions from chemically active airglow layers at mesopause altitudes are readily monitored by ground and space based low light imaging systems (Taylor, 1997). The NASA Global-scale Space-based observations of twilight airglow is conducted by using the

Limb and Disk instrument. It is an ultraviolet imager and spectrograph that observes light from the upper atmosphere of the Earth. At night but near twilight, Solomon et al. (2020) realized broad regions of faint emissions of airglow light, particularly during winter. These are caused by electrons that are created by ionization on the dayside, and then transported along field lines from magnetically conjugate areas in the other hemisphere, where those areas are still illuminated.

The observation sight, R. K. Nagar, Kolhapur, Maharashtra, India is located at $16^0$39’42.2” N, $74^0$14’20.8” E and 613 meters elevation. This sight is free from large-scale industrial and urban activities. It is mainly surrounded by residential area and agricultural land. The observational sight is free from urban light pollution. It belongs to Class-4 according to Bortle Dark Sky Scale. Its sky description comes under the Rural/Suburban transition zone (given by light pollution map). According to Indian climatic zone map this sight comes under ‘Tropical wet & dry’ climate zone (based on the Köppen climate classification).

2. INSTRUMENTATION AND METHODOLOGY

The instrument, Semiautomatic Twilight Photometer, was newly designed, developed and installed at Kolhapur, Maharashtra, India. The system is a ground based passive remote sensing technique mainly used to monitor the vertical distribution of the atmospheric aerosols. It is a simple and inexpensive but very sensitive instrument and hence operated continuously for monitoring the day-to-day observations, at any place.

The semiautomatic twilight photometer consists of a simple experimental set up. It comprises of a pleno-convex lens of diameter 15 cm having a focal length of 35 cm. A red band-pass glass filter peaking at 660 nm with a half bandwidth of about 50 nm and transmission ≥ 85% is used. The aperture of 0.6 cm diameter placed at the focal length of convex lens, provides approximately 1^0 field of view. The detector is a photomultiplier tube (PMT-R669). The PMT requires high voltage supply of about 600V. The output signal (current) of the PMT, used for detecting the light intensity during the twilight period, is very low. It is of the order of nanoamperes to microamperes. The newly invented Fast Pre-amplifier amplifies the amplitude or strength of this low signal. The more details about this modified instrument are enclosed elsewhere (Mane & Mane 2021). The digital multimeter, Rishcom-100, having an adapter can store the data automatically for every 10 seconds in the form of date, time and intensity in Volts. During evening, the twilight photometer is operated for a time spell of ~90 minutes after the local sunset and during morning; it is operated ~90 minutes before the sunrise. It is able to probe in the atmosphere from 6 km to 350 km.

Observed time ‘t’ and intensity ‘I’ are two important parameters of the twilight technique, constitutes raw data. This raw data was utilized for the calculation of shadow height (h). Further, it is used for the analysis of ‘(1/I) (dI/dh)’ value, where ‘I’ is the observed intensity, ‘dI’ and ‘dh’ are the differences in intensities and shadow heights respectively observed at time ‘t’ and ‘t+dt’. Shah (1970) described the method for calculating the earth's geometrical shadow height (h). Thus, the earth's geometrical shadow height (h) is defined as the vertical height from the observer on the surface of the earth, where the solar ray grazing the surface of the earth meets the line of slight. Therefore,

$$h = R\,[\text{secant}\,(\delta) - 1] \qquad \ldots (1)$$

Here, ‘R’ is radius of earth and ‘δ’ is sun's depression below observer’s horizon.

Thus, profiles of Altitude (shadow height, h) against ‘(1/I) (dI/dh)’ value obtained during twilights were plotted. Many of such graphs were studied and discussed the results. This is being ground based passive remote sensing instrument, the sky needs to be clear at morning and evening twilight observations. It is important to note that being a tropical location, the availability of optically clear sky makes the statistics biased. The maximum number of cloud free morning and evening twilights were monitored.

3. RESULTS AND DISCUSSION

Principally, profiles of Altitude against '(1/I) (dI/dh)' value obtained during twilights were used for study of vertical distribution of aerosols. Hence, they are called as vertical profiles of aerosols. Figure-1 represents aerosol vertical profile free from twilight airglow activities. The rate of change of red light due to the twilight airglow would shows narrow intense peaks on the vertical profiles of aerosols. The intensity of these lines is ~600% to 1000% higher than typical natural twilight glow due to aerosols. In semiautomatic twilight photometer a red glass filter peaking at 660 nm with half bandwidth of about 50 nm is used. Therefore, the twilight glow lines having wavelengths in between 6100 Å and 7100 Å were detected by this instrument. In the following subsections, twilight airglow red emissions are discussed in the descending order of their altitudinal existences.

The airglow normally occurs in layers at varying altitudes above the earth's surface, the height or heights and the thicknesses of the layers depending on the production mechanism and therefore on such factors as the composition and its variation with height. The intensity of emission lines may be patchy in nature and the size of these patches may be of the order of thousands of kilometers (Silverman, 1970). Twilight offers an opportunity to observe resonant scattering of sunlight on layers. As the Earth's shadow scans through the layers, the changes of intensity allow their heights to be measured. The fact of the attitudinal separation of the Twilight photometric data is utilized to determine the altitude and thickness associated with the bright airglow layers in the existing work. Megrelishvili (1958), made intensity measurements of the twilight glow using twilight photometer, in U.S.S.R, in a direction 70° from the zenith in the Sun's meridian plane, at two different wavelengths, one at 9400 Å and the other at 5270 Å. He did not observe any maximum on the curves of '1/I (dI/dh)' against 'h' for 5270 Å but observed two maxima, one at about 47 km and the other at about 100 km for 9400 Å.

All the figures in-between Figure-1 to Figure-9 demonstrates the profiles of 'Altitude' against '(1/I) (dI/dh)' value. For each of these graphs, X-axis symbolizes '(1/I) (dI/dh)' value and Y-axis indicates 'Altitude in kilometers'. Here 'E' stands for graph of Evening twilight and 'M' denotes graph of Morning twilight. The aerosol vertical profiles within altitudinal intervals of 6km - 360 km are considered here. Altitude of twilight airglow emission peak and thickness is mentioned for each graph.

3.1. Ionized Nitrogen (N_2) emission

According to Hunten (1967) photoelectrons could be descending from great heights where solar radiation is still intense, and ionizing the nitrogen (N_2) at a fixed height of around 300 km. The spectrum of ionized nitrogen (N II) is built up from 6482.05 Å & 6610.56 Å and 6482.70 Å emission from (N I) (Fowler & Freeman, 1927).

Figure-2 shows twilight airglow emission of ionized nitrogen. Excited nitrogen molecules and nitrogen molecular ions produce red lines. One perceptible point was that for the entire three years, frequency of N_2 emission was lowest for the period free from strong meteor activities; whereas maximum for the month of December and January, the period followed by two strong meteor activities Geminids (14th December) & Quadrantids (3rd January) and several weak & medium meteor activities. N_2 emission for month of December showed two broad and intense peaks during 14th December & 19th December, 2010 during active period (Dec 13-Dec 16) of Geminids meteor activities. A quite different picture was observed during month of January; at the time of several weak & medium meteor activities. During month of January, Twilight photometer detected closely spaced two emissions with narrow thickness above 300 km. The lower layer is thicker than the upper one. The height and thickness of both the emissions showed day-to-day variability. The intensity of emissions was lower during January as comparison with that of December emissions.

Our observations for ionized Nitrogen (N_2) emissions are supported by several earlier researchers. Jenniskens (2004) reported the discovery of the N_2^+ *A-X* Meinel band in the 780–840 nm meteor emission from two Leonid meteoroids. The N_2 electronic transition appears readily in most discharges containing air or nitrogen. It occurs in emission spectra from the Earth's upper atmosphere, associated with phenomena including aurorae [Ashrafi et al. 2009] and sprites [Bucsela et al. 2003 & Luque et al. 2011]. Western et al. 2019 recorded N_2 emission from 9000 to 15700 cm−1 i.e. from ~6369 Å to 11111Å at Doppler-limited resolution, on a Fourier transform spectrometer. The research effort described by Thomas J. Immel et al. (2020); indicated that photoelectron populations stimulate emissions of N_2 are easily observed from space-based platforms. The dissertation by Murray Donald, (2007) and recent work by Eastes, (2000) focused on the N_2 Lyman-Birge-Hopfield (LBH) band (a1Πg−X1Σg+) emissions from the Earth's aurora and daytime airglow. They used them for remote sensing of thermospheric

temperature profiles. N_2 LBH emissions occurring in the dayglow radiate in the UV between 1270 and 2400 Å.

3.2. Forbidden Red Doublet of oxygen emission (6300 Å & 6364 Å)

It is well known that [OI] 630 nm emission in the nighttime originates mostly from the bottom side of the F-region at about 250 km altitude in low and middle latitudes by the dissociative recombination process (Mukherjee et al. 2008) given by:

$$O_2 + e \rightarrow O + O* (^1D);$$

$$O* (^1D) \rightarrow O + h\nu (\lambda = 630 \text{ nm}).$$

The rate of this reaction is nearly proportional to the rate of recombination in the F_2 layer (Mukherjee et al. 2000). In the thermosphere around 250 km, the 630 nm emission intensity strongly depends on the density of O ion, O molecule and electrons in the F-region. In addition, the intensity decreases when the ionospheric layer moves up and vice versa (Parihar et al. 2012).

Figure-3 shows twilight airglow emission due to excited oxygen atoms. In this study oxygen emission red lines of 6300 Å & 6364 Å are deteced in between the altitudes 200 and 300 km. Intensity of oxygen red emission is moderate to high with width 4 to 10 km. The red emission of atomic oxygen (OI 630 nm) is the brightest discrete line observed in the low-latitude twilight airglow. Our observations of twilight airglow emission due to excited oxygen atoms are analogues to the observations made by Mukherjee G. K. (2006) at the same station. He used a CCD based all-sky imaging system to monitor various nightglow emissions (OI 630-nm, OI 557.7- nm, OI 777.4-nm, Na (589.3-nm) and hydroxyl (OH) airglow) at the same low latitude station, Kolhapur (16.8°N, 74.2°E) in India to study the characteristics of night airglow variations observed during the period of a moderate/weak geomagnetic storm on February 5, 2000. He observed that the maximum altitudes of OI 630.0-nm and OH Meinel band emissions are 250 and 87 km, respectively.

Former and recent airglow scientists all over the world studied mainly about emission of atomic oxygen (OI 630 nm) & OH. Hays et al. (1969) have measured the temperature by interferometric means using the 6300 A [O1] line during a magnetic storm in 1968 at Ann Arbor, Mich. (geogr. lat. 42° 16 N, long. 83° 44' W). During a part of the time a stable auroral red arc (SAR) was present. They found no detectable temperature difference within and outside the arc.

They found also that the temperatures responded to the changes in magnetic activity rapidly, with a phase shift of the order of 3 hours. The peak emission rate of 630-nm airglow occurs at 250–260 km [Kubota et al., 2000; Ogawa et al. 2002]. The dissociative recombination of ions and electrons is the main source of OI 630 nm emission in the F region. Variations in their intensities are closely correlated with variations in the electron concentration and neutral composition at these altitudes (Leonovich et al. 2011).

3.3. Emission involved in formation of nitric oxide (NO) molecule

The main components of air in the thermosphere include helium, atomic nitrogen, and atomic oxygen. Nitric oxide (NO) is one of the major background constituents in the lower thermosphere and its presence can have direct and indirect consequences to Earth's radiation budget. NO densities vary with solar and geomagnetic activity. Solar radiation (soft X-rays and UV) is responsible for dissociating the strong N_2 and O_2 bands. The total number density of SOFIE observations show the NO reservoir to be at approximately 100 km, with changes throughout the year in the altitude of the maximum density. An NO reservoir is present between 100 and 110 km altitude (Siskind et al., 1998; Sheese et al., 2013) and the main production processes of NO involve the interaction of ground-state and excited nitrogen with molecular oxygen, while destruction occurs primarily via ground-state nitrogen, ionized molecular oxygen and solar UV radiation (Barth, 1995). Nitric oxide (NO) molecule such formed is not stable (it is a very reactive molecule) as it has an odd number of electrons. It rapidly oxidizes to form nitrogen dioxide (NO_2). In this process, a photon is emitted. This photon may have any of several different wavelengths' characteristic of nitric oxide molecules. NO & NO_2 such formed are rapidly interconverted in the sunlit atmosphere on a timescale of seconds.

Figure-4 shows twilight airglow emission caused by formation of a molecule of nitric oxide (NO). This is the brightest emission in the passband of the present study. The peak of the emission is located between 110 & 120 km. The thickness of the emission is very low (~1.5 km). Hendrickx et al. 2018 showed the mean NO density between 90 and 140 km altitude.

3.4. Metallic emission (Sodium and Lithium emission)

The formation of distinct layers of metal atoms such as sodium, Lithium etc. around 90 km takes place due to the ablation of meteoroids in the upper atmosphere [Plane, 2003]. The sodium layer located at 80–105 km and having a depth of about 5 km refers to a layer within the

Earth's mesosphere of unbound, non-ionized sodium atoms. Atoms of sodium in this layer are typically in an excited state, and radiate four red lines between 6500 and 6700 Angstroms. The resulting radiation is one of the sources of airglow (Ageorges et al. 1999).

Other metallic species that can create airglow in the atmosphere are lithium (Li) (Donahue, 1959). Li emission line near 6708 Å has been reported by Delannoy and Weill (1958) to be present on twilight spectrograms. This emission is the impact of dissociative excitation given by Henrikson (1980):

$$LiO^* + O \rightarrow Li^* + O2$$

$$Li^* \rightarrow Li + h\nu\ (6708\ Å)$$

Figure-5 shows twilight airglow metallic emissions of sodium and lithium. Twilight emissions of alkali metals like Lithium (at 671nm) and Sodium (between 650 and 670 nm) are located form ~80 to 105 km. These emissions were observed in almost all months of the observation period. One significant thing to note here is that very narrow and brighter emission lines were detected after strong meteor activities. However, the emissions observed followed by weak & medium meteor activities were boarder but weaker in intensity. This indicates ZHR dependency of alkali metals emissions. [ZHR: Zenith Hourly Rate, the average maximum number of shower meteors visible per hour if the radiant is located exactly overhead]. [More details regarding meteor activities are enclosed elsewhere (Mane & Mane, 2021)].

Gu et al. (1995), obtained Sodium density profile with airborne Na LIDAR with peak density at 94 km with Full-Width Half-Maximum (FWHM) of 0.6 km. Those profiles are similar to our twilight airglow profiles. This hypothesize that twilight airglow profiles obtained using Twilight Photometer can provide information about density of relevant components in the Earth's atmosphere at the particular altitude.

The study of twilight airglow metallic emissions is having very long history. Jones (1959) conducted observations of twilight airglow for lithium emission. They exhibit completely different seasonal behavior. In the extra tropics' Na varies annually, with a pronounced wintertime maximum and summertime minimum. However, K varies semiannually with a small summer time maximum and minima at the equinoxes (Plane, J. et al. 2014). Sullivan & Hunten (1964) used a birefringent filter photometer to measure the weaker twilight emissions due to free

lithium and potassium atoms. They used an interference wedge photometer to monitor the twilight sodium emission simultaneously. They observed that at twilight lithium emission has been found, showing a correlation with the occurrence of the Leonid meteor shower. Sodium is also having origin from meteorites. According to them, the maximum concentration of lithium occurs at 80 km, approximately 11 km below the sodium peak, while the maximum concentration of potassium occurs at about the same height as the sodium peak. Gault et al. (1969) made Twilight observations of upper atmospheric sodium, potassium, and lithium for over one year. Their results indicate that sodium and lithium layers are both at about the same height of around 90 km and a lower height of about 85 km was obtained for the potassium layer.

The dayglow height profile is also of interest, especially in connection with the photochemistry of sodium. Hunten & Wallace (1967) obtained two good profiles of the emission for comparison with twilight measurements using sodium dayglow photometers flown on Aerobee rockets. They observed that in June, the twilight and daytime abundances were the same; the vertical distributions agreed fairly well. In April, the daytime abundance was greater by a factor of about 1.45; the heights were again nearly the same. Midya et al. (2001) reported that both chemical kinetically and practically, Li 6708 Å line intensity decreases proportionally with dramatic depletion of ozone at two Antarctic survey stations.

3.5. Hydroxyl (OH) band emissions

OH, shows red twilight enhancement at 6329 Å. The height of peak emission layer is ~90km. A possible mechanism for hydroxyl emission was first proposed by Bates and Nicolet (1950):

Chemiluminescence cycle

$$H + O_3 \rightarrow OH\ (v \leq 9) + O_2,$$

$$OH + O \rightarrow O_2 + H.$$

The vibration-rotation bands of OH are, the most intense emissions of the night airglow. Though controversy exists, the most favored mechanism at this time is that proposed by (Silverman, 1970):

$$H + O_3 \rightarrow OH^* + O_2$$

According to Bellisario et al. (2020), the OH vibrational states originate from the reaction between H and O_3 and the ozone photodissociates during the day. Vibrational-rotational levels at ~85 km, OH is very short-lived produced by

$$O_3 + \gamma \rightarrow O + O_2,\ O + H_2O \rightarrow 2OH.$$

Figure-6 shows OH twilight airglow layer. In the present study it was noticed that vibrationally and rotationally excited OH radicals emit red line in a narrow layer centered at ~83-87 km. Similar results are reported by Ghodpage et al. (2013, 2014) at the same station Kolhapur. They made simultaneous MLTP measurements of mesospheric OH night airglow emissions from two stations, Gadanki (13.5° N, 79.2° E) and Kolhapur (16.8° N, 74.2° E), India during February-March 2010. They observed that the observed nighttime OH emission profile shows the peak of emission at ~ 85 km in Kolhapur and at ~ 90 km in Gadanki in the corresponding months.

Supporting studies are presented by many investigators. Shefov (1968, 1969) has found periodic variations in the rotational temperature of the hydroxyl emission for as long as 30 days after the magnetic storm commencement. For the hydroxyl emission, the energy release involved in these radiations on a planetary scale was of the same order as that of the entire energy of the geomagnetic storm. The production of OH* has a peak at altitudes of 80-90 km above ground. Above this height, the production is limited by the rapid fall off in ozone concentration and below it is limited by the onset of rapid quenching of the excited products by collisions more frequent at the higher atmospheric pressures. The balance between the two processes creates the narrow OH airglow layer (Chamberlain, 1962). A more detailed study by Yee et al. (1997) using HRDI (High Resolution Doppler Imager) results from UARS (Upper Atmosphere Research Satellite) showed that the peak altitude of the night time OH emissions could occur anywhere in the range 86–91 km. Rocket measurements by Baker & Stair (1988) found a normal peak altitude of ~87 km and a width of 8 km. She & Lowe (1998) and Oberheide et al. (2006) confirmed that this interpretation is an accurate assessment of the time averaged height and width of the layer.

3.6. Emission of RED Sprites

Sprites are large-scale electrical discharges that occur high above a thunderstorm or cumulonimbus clouds, giving rise to a quite varied range of visual shapes. They are triggered by

the discharges of positive lightning between the thundercloud and the ground. Sprites are optical emissions in the mesosphere mainly at altitudes 50–90 km. They are caused by the sudden re-distribution of charge due to lightning in the troposphere that can produce electric fields in the mesosphere in excess of the local breakdown field. The resulting optical displays can be spectacular (Boccippio et al. 1995).

Earlier scientists described that emissions of sprites are related a thunderstorm or cumulonimbus clouds or lightning. In the present study it was observed that emission of red sprites during twilight appeared at the arrival or departure phase of different types of middle level and low-level clouds. They emit red lines in a narrow layer centered at altitudes 50–75 km with moderate to high intensity. This is being tropical station different types of clouds were found in between the days with clear skies. During the observations of 2009-2011; visual observations of different types of clouds were noted down. Figure-7 shows some examples of emission of red sprites during existing twilight studies.

It was often observed that sprites were arrived at the withdrawal phase of large quantity of Nimbostratus clouds. For example: We seen Nimbostratus clouds during 9^{th}- 12^{th} January 2009 and the morning twilights of 13-01-2009 reflected red sprites with wide-rang peak emission at altitude 55.53 km. Same type of observation reported in case of sprites emissions of the morning twilights of 28-04-2009. Here, during previous two days 26^{th} & 27^{th} April 2009, sky was occupied with Nimbostratus clouds. Further, sprites appeared during morning twilight of 25-1-2009 and at the same time Nimbostratus clouds looked at west horizon.

Sometimes sprites were detected at arrival of cumulonimbus clouds. For example: the evening twilights of 15-02-2009 acquired intense narrow peak of red sprites emission at altitude 51.26 km and on the next day during morning cumulonimbus clouds visual at west horizon. They were also present at east horizon on the same day of evening twilight observation of narrow sprites with very large intensity during 06-04-2009.

Stratocumulus clouds also take part in red sprites emission. At the afternoon of 18^{th} March 2009 sky was filled with stratocumulus clouds. By evening, the winds had blown away the clouds, and clear sky observations produced red sprites emission at altitude 76.18 km. Further, sprites seemed during evening twilights on a day when the morning dew fell. For

example: weaker & narrow sprites during evening twilights of 22-11-2009. Large quantity of dew fell during morning at the same day as this is the winter season in India.

Fair weather cumulous clouds play important role in the sprite formation. Sprites formed on both onset and offset of fair-weather cumulous clouds. Two of such examples furnished herewith. Sprites of 23-01-2010 formed at onset and those of 26-02-2010 at offset of fair-weather cumulous clouds.

Our observations of altitude of sprites are well agreements with those with earlier observations. According to Lyons & Schmidt (2003), sprites have since been witnessed thousands of times. Sprites often occur in clusters, lying 50 kilometers to 90 kilometers above the Earth's surface. Sprites' images were recorded by Nielsen et al. (2013) at 1 ms resolution occurring in a highly structured mesosphere. These images revealed several new properties about sprite. Very recently, NASA astronauts took a new set of pictures from the International Space Station during night time in the frame of the NASA Crew Earth Observations program, giving a new opportunity to observe in color sprites and their parent lightning flashes. The sprite vertical structure extends from 55 to 85 km in the red filter image (Jehl, 2013).

3.7. Multilayered Twilight airglow red emissions

Some times more than one twilight airglow red lines in the pass-band of twilight photometer had visible on the same aerosol vertical profile. Two such examples are herewith. Figure-8 shows two different types of twilight airglow red emissions on 01-02-2011. Red sprite emission having peak altitude at 55.25 km with thickness of 1.62 km and closely spaced two emissions of ionized Nitrogen (N_2) with narrow thickness above 340 km are noticed here. As usual the lower layer is thicker than the upper one. Mid of January to first week of February is the coldest period during the winter in India. Hence it is the period of morning dew fall and fog formation. Such an atmospheric activities are related to the red sprite emission.

Figure-9 demonstrated three-layered twilight airglow red emissions on 09-02-2009; one Hydroxyl (OH) emission at 81.13 km with thickness 6.86 km, second one is Metallic emission (Altitude of Peak: 88.75 km; Thickness: 7.17 km) and third emission of Nitric Oxide (NO) formation (Altitude of Peak: 140.84 km; Thickness: 5.53 km). All these three emissions are related to the metallic layers formed due to the ablation of meteoroids in the upper atmosphere.

Several weak and medium meteors are active in the ending of January & beginning of February. This may be the reason for multilayered emission.

These observations of multilayered twilight airglow emissions emphasize the distinguished twilight airglow exploring feature of Twilight photometer. Other known instruments are unable to provide information about multilayered airglow emission at one glance.

4. SUMMERY AND CONCLUSION

Maximum of all kinds of red twilight airglow emissions except red sprites were detected during the months of mid of December to mid of February, the period free from contamination due to different types of clouds. The emissions from the mesosphere and the lower thermosphere have been identified with some certainty, along with the major excitation processes, a fruitful possibility exists for detailed long-term study from the ground. Few if any developments of technique are needed; the main lack is a wide distribution of observing stations, with continuing programs. Moreover, because of the inherent variability and poor weather, it is necessary to accumulate several years of data at any station before the typical behavior can be deduced. Hence it is needed to study the maximum variability in spatial and temporal distribution and notice variation in chemical nature over observation regions. Because of these phenomena, various atmospheric oscillations were observed.

This study highlights the important characteristic of Twilight photometer, producing statistics about multilayered airglow emissions at one glance. However, it is not sufficient to study altitudinal separation of these lines only. As twilight airglow lines are strong functions of their wavelengths; it is essential to conduct the multi-spectral twilight photometer measures. Hence, it is essential to use filters peaking at different wavelengths with narrow pass-band for detail study of twilight airglow emissions. Twilight photometer can provide an opportunity to change the filters very easily.

The main aim of this study is to highlight the conspicuous capability of Semiautomatic twilight photometer to study the twilight airglow emission lines. Twilight photometer, although currently seldom used, is still a very effective and the most appropriate ground based passive remote sensing tool for long-term monitoring of atmospheric components and different atmospheric parameters in a wide range of altitudes for day-to-day basis. It is an efficient system having a simple and inexpensive underlying principle of operations, yet exhibits extremely accurate and precise usage and can be operated by even a person of average skill. However, it can be seen that the resultant data was consistent with nearest peer technologies, such as LIDARs, Balloon-Borne instruments, rocket measurements, satellite observations etc. It is the first attempt in India to obtain the twilight airglow observations using Twilight photometer.

ACKNOWLEDGMENT

Author is grateful to the authorities, Fergusson College, Pune, for the encouragement during the course of this work. Further deep sense of gratitude goes towards DST, Women Scientist Scheme-A (WOS-A), India, for providing the Fellowship and funds for the development of twilight photometer and potential research work.

REFERENCES

1. Jadhav D. B., Padma Kumari B. & Londhe A. L., (2000). A review on twilight photometric studies for stratospheric aerosols. *Bulletin of Indian Aerosol Science & Technology Association*, vol.13, pp. 1–17.
2. Bellisario Christophe, Pierre Simoneau, Philippe Keckhut, and Alain Hauchecorne, (2020). Comparisons of spectrally resolved nightglow emission locally simulated with space and ground level observations. *J. Space Weather Space Clim*., vol.10, 21. https://doi.org/10.1051/swsc/2020017.
3. Meinel, I. A. B., (1950). OH emission bands in the spectrum of the night sky. *The Astrophysical Journal*, vol. 111, p. 555. https://doi.org/10.1086/145296.
4. Chamberlain J W, Roesler F L., (1955). The OH bands in the infrared airglow. *The Astrophysical Journal*, vol. 121, p. 541. https://doi.org/10.1086/146015.
5. Baker D J, Stair A T Jr., (1988). Rocket measurements of the altitude distributions of the hydroxyl airglow. *Phys. Scr.*, vol. 37, pp. 611–622. https://doi.org/10.1088/0031-8949/37/4/021.
6. Burrage M D, Arvin N, Skinner W R, Hays P B., (1994). Observations of the O_2 atmospheric band nightglow by the high-resolution Doppler imager. *Journal of Geophysical Research*, vol. 99, pp. 15017–15024. https://doi.org/10.1029/ 94JA00791.
7. Marsh D R, Smith A K, Mlynczak M G, Russell J M., (2006). SABER observations of the OH Meinel airglow variability near the mesopause. *Journal of Geophysical Research (Space Phys)*, vol. 111(A10). https://doi.org/10.1029/2005JA011451.
8. Shepherd G G, Thuillier G, Cho Y-M, Duboin M-L, Evans W F J, et al., (2012). The wind imaging interferometer (WINDII) on the upper atmosphere research satellite: A 20-year perspective. *Rev Geophys*, 50: RG2007. https://doi.org/10.1029/2012RG000390.
9. Bellisario C, Keckhut P, Blanot L, Hauchecorne A, Simoneau P., (2014). O_2 and OH night airglow emission derived from GOMOSEnvisat instrument. *J Atmos Ocean Technol*., vol. 31(6), pp. 1301–1311. https://doi.org/10.1175/JTECH-D-13-00135.1.
10. Hunten, D. M., (1967). Spectroscopic Studies of the Twilight Airglow. *Space Science Reviews*, vol. 6 (4), pp. 493-573. 1967SSRv....6...493H.

11. Swider, Jr. W., (1969). Upper Atmospheric Emission Processes, in McCormac and Omholt (eds.), pp. 367-382.
12. Pick, D. R., E. J. Llewellyn & A. Vallance Jones, (1971). Twilight Airglow Measurements of the OH and O_2 Bands by Means of Balloon-Borne Instruments, *Canadian Journal of Physics*, vol. 49 (7). https://doi.org/10.1139/p71-108.
13. Moreels G., A. Vallance Jones, J. E. Blamont, (1973). A Balloon Study of the OH Airglow Emission from Evening Twilight to Sunrise. *Canadian Journal of Physics*, vol. 51 (9), pp. 888-893. https://doi.org/10.1139/p73-120.
14. Moos, H. W. & W. G. Fastie, (1967). Rocket photometry of the far UV twilight airglow. *Journal of Geophysical Research*, vol.72(21), pp 5165–5171.
15. Taylor, M. J., (1997). A review of advances in imaging techniques for measuring short period gravity waves in the mesosphere and lower thermosphere. *Adv. Space Res*., vol. 19, pp. 667–676.
16. Solomon Stanley C., Laila Andersson, Alan G. Burns, Richard W. Eastes, Carlos Martinis, William E. McClintock, Arthur D. Richmond, (2020). Global-Scale Observations and Modeling of Far-Ultraviolet Airglow During Twilight. *Journal of Geophysical Research-Space Physics*, vol.125(3). https://doi.org/10.1029/2019JA027645.
17. Mane Pratibha B. & Mane Dhairyasheel B., (2021), Study of Aerosol vertical distribution during Meteor showers of January 2009, *Journal of Atmospheric and Solar-Terrestrial Physics*, vol. 213, p. 105511. https://doi.org/10.1016/j.jastp.2020.105511.
18. Shah, G. M., (1970). Study of aerosol in the atmosphere by twilight scattering. *Tellus*, vol. 22, pp 82-93.
19. Megrelishvili T G, (1958). The possibility of investigating aerosol layer by twilight photometer. *Ind. J. Meteor. & Geophy*., vol. 9, p. 271.
20. Rafferty John P., (2015). Airglow. Encyclopedia Britannica. https://www.britannica.com/science/airglow.
21. Chattopadhyay R and S K Midya, (2006). Airglow emissions: fundamentals of theory and experiment. *Indian J. Phys*. 80 (2), pp. 115-166.
22. Agashe, V V, (1987). Airglow Studies in India. *Indian Journal of Radio & Space Physics*, vol. 16, pp. 84-101
23. Hunten, D. M., (1967). Spectroscopic Studies of the Twilight Airglow. *Space Science Reviews*, vol. 6(4), pp. 493-573. 1967SSRv....6..493H.
24. Fowler Alfred & Freeman L. J., (1927). The spectrum of ionised nitrogen (N II). *Proc. R. Soc. Lond*., vol. A 114, pp 662–689. http://doi.org/10.1098/rspa.1927.0068
25. Mukherjee G. K., L. Carlo, and S. H. Mahajan, (2000). 630 nm nightglow observations from 17°N latitude, *Earth Planets Space*, vol. 52, pp 105–110. https://doi.org/10.1186/BF03351618.
26. Mukherjee G. K. & D. J. Shetti, (2008). Plasma drift motion in the F-region of the ionosphere using photometric nightglow measurements. *Indian Journal of Radio & Space Physics*, Vol. 37 (4), pp. 249-257.

27. Parihar Navin, B A Kakad& G K Mukherjee, (2012). Nightglow observations of Ol 630 nm emission during the beginning of solar cycle 24 over 25°N, India. *Indian Journal of Radio & Space Physics*, vol 41, pp 155-16l.
28. Siskind, D. E., Barth, C. A., and Russell, J. M., (1998). A climatology of nitric oxide in the mesosphere and thermosphere. *Adv. Space Res.*, vol. 21, pp. 1353–1362. https://doi.org/10.1016/S0273-1177(97)00743-6.
29. Sheese, P. E., Strong, K., Gattinger, R. L., Llewellyn, E. J., Urban, J., Boone, C. D., and Smith, A. K., (2013). Odin observations of Antarctic nighttime NO densities in the mesosphere-lower thermosphere and observations of a lower NO layer. *Journal of Geophysical Research-* Atmospheres, vol. 118, pp. 7414–7425. https://doi.org/10.1002/jgrd.50563.
30. Barth, C. A., (1995). Nitric Oxide in the Lower Thermosphere, in: The Upper Mesosphere and Lower Thermosphere: A Review of Experiment and Theory, edited by: Johnson, R. M. and Killeen, T. L., Vol. 87, Geophysical Monograph Series, 225–233, American Geophysical Union, Washington, D.C., https://doi.org/10.1029/GM087p0225.
31. Plane, J. M. C. (2003). Atmospheric chemistry of meteoric metals, *Chem. Rev.*, vol. 103(12), pp. 4963–4984.
32. Ageorges, N.; Hubin, N.; Redfern, R.M. (1999). Atmospheric Sodium Column Density Monitoring, ESO Conference and Workshop Proceedings (Garching: European Southern Observatory) 56, Bibcode:1999ESOC...56....3A, retrieved 2011-09-04.
33. Donahue, T. M. (1959). "Origin of Sodium and Lithium in the Upper Atmosphere". Nature. Vol.183 (4673), pp. 1480–1481. Bibcode:1959Natur.183.1480D. doi:10.1038/1831480a0.
34. Delannoy, J. and Weill, G., (1958). *Compt. Rend. Acad. Sci*. 246, 2925.
35. Henrikson, A., (1980). The Geographical "Mental Maps" of American Foreign Policy Makers. International Political Science Review / Revue Internationale De Science Politique, 1(4), 495-530. Retrieved May 21, 2021, http://www.jstor.org/stable/1600751.
36. Bates D R, M Nicolet, (1950). The photochemistry of atmospheric water vapor. *Journal of Geophysical Research*, vol. 55(3), pp. 301-327.
37. Silverman S. M., (1970). Night airglow phenomenology, *Space Science Reviews*, vol. 11, pp. 341-379.
38. Bellisario Christophe, Pierre Simoneau, Philippe Keckhut and Alain Hauchecorne, (2020). Comparisons of spectrally resolved nightglow emission locally simulated with space and ground level observations. *J. Space Weather Space Clim.*, vol. 10, p. 21. https://doi.org/10.1051/swsc/2020017.
39. Boccippio, D. J.; Williams, E. R.; Heckman, S. J.; Lyons, W. A.; Baker, I. T.; Boldi, R. (1995). "Sprites, ELF Transients, and Positive Ground Strokes". *Science*, vol. 269 (5227), pp. 1088–1091.

40. Jenniskens P, Laux C O, Schaller E L (2004). Search for the OH (X 2 Π) Meinel band emission in meteors as a tracer of mineral water in comets: Detection of N_2^+ (A-X). *Astrobiology*, vol. 4, pp. 109-21.
41. Ashrafi M, Lanchester BS, Lummerzheim D, Ivchenko N, Jokiaho O (2009). Modelling of N_2 1 P emission rates in aurora using various cross sections for excitation. *Ann Geophys*., vol. 2, pp. 2545-53.
42. Bucsela E, Morrill J, Heavner M, Siefring C, Berg S, Hampton D, et al. (2003). N_2(B 3 Πg) and N_2 + (A 2 Πu) vibrational distributions observed in sprites. *Journal of Atmospheric and Solar-Terrestrial Physics*, vol. 65, pp. 583-90.
43. Luque A, Gordillo-Vazquez F J, (2011). Modeling and analysis of N2(B 3 Πg) and N_2(C 3 Πu) vibrational distributions in sprites. *Journal of Geophysical Research-Space Physics*, 116.
44. Western Colin, Luke Carter-Blatchford, Patrick Crozet, Amanda J. Ross, Jérôme Morville, et al. (2018). The spectrum of N_2 from 4,500 to 15,700 cm^{-1} revisited with PGOPHER. *Journal of Quantitative Spectroscopy and Radiative Transfer*, vol. 219, pp.127-141. ff10.1016/j.jqsrt.2018.07.017ff. ffhal-02121597f
45. Thomas J. Immel , Richard W. Eastes , William E. McClintock , Steven B. Mende , Harald U. Frey , Colin Triplett and Scott L. England (2020). Daily Variability in the Terrestrial UV Airglow. *Atmosphere*, vol. 11, p. 1046; doi:10.3390/atmos11101046.
46. Murray Donald, (2007). Modeled and Observed N_2 Lyman-Birge-Hopfield Band Emissions Earth's Dayglow: A Comparison, Electronic Theses and Dissertations, 2004-2019. 3274. https://stars.library.ucf.edu/etd/3274
47. Eastes R.W., (2000). Emissions from the N_2 Lyman-Birge-Hopfield bands in the earth's atmosphere. *Physics and Chemistry of the Earth, Part C: Solar, Terrestrial & Planetary Science*, vol. 25(5–6), pp. 523-527. https://doi.org/10.1016/S1464-1917(00)00069-6.
48. Mukherjee, G.K., (2006). Airglow and other F-layer variations in the Indian sector during the geomagnetic storm of February 5–7, 2000. *Earth Planet Space*, vol. 58, pp. 623–632. https://doi.org/10.1186/BF03351960
49. Hays, P. B., Nagy, A. F., and Roble, R. G., (1969). 'Interferometric Measurements of the 6300 Å Doppler Temperature during a Magnetic Storm', *Journal of Geophysical Research*, vol. 74, pp. 4162-4168.
50. Kubota, M., K. Shiokawa, M. K. Ejiri, Y. Otsuka, T. Ogawa, T. Sakanoi, H. Fukunishi, M. Yamamoto, S. Fukao, and A. Saito, (2000). Traveling ionospheric disturbances observed in the OI 630-nm nightglow images vver Japan by using a multipoint imager network during the FRONT campaign, *Geophys. Res. Lett*., vol. 27(24), pp. 4037 – 4040, doi:10.1029/2000GL011858.
51. Ogawa, T., N. Balan, Y. Otsuka, K. Shiokawa, C. Ihara, T. Shimomai, and A. Saito, (2002). Observations and modeling of 630 nm airglow and total electron content associated with traveling ionospheric disturbances over Shigaraki, Japan, *Earth Planets Space*, vol. 54, pp. 45–56.

52. Leonovich L.A., A.V. Mikhalev, V.A. Leonovich, (2011). Upper atmosphere nightglow disturbances during the geomagnetic storm of December 15, 2006 over Eastern Siberia. *Atmospheric and Oceanic Optics*, vol. 24(6), pp. 579–583. DOI: 10.1134/S1024856011060091.
53. Hendrickx, K., Megner, L., Marsh, D. R., and Smith-Johnsen, C., (2018). Production and transport mechanisms of NO in the polar upper mesosphere and lower thermosphere in observations and models, *Atmos. Chem. Phys*., vol. 18, pp. 9075–9089. https://doi.org/10.5194/acp-18-9075-2018.
54. Jones, A., (1959). Observations of the Lithium Lines in the Twilight Airglow in the Northern Hemisphere. *Nature*, vol. 183, pp. 1315–1316. https://doi.org/10.1038/1831315b0
55. Plane, J., Feng, W., Dawkins, E., Chipperfield, M., Höffner, J., Janches, D., & Marsh, D. (2014). Resolving the Strange Behavior of Extraterrestrial Potassium in the Upper Atmosphere. *Geophysical Research Letters*, vol. 41, pp. 4753-4760. DOI: 10.1002/2014GL060334.
56. Sullivan H. M. & D. M. Hunten, (1964). Lithium, sodium, and potassium in the twilight airglow. *Canadian Journal of Physics*, vol. 42 (5), pp. 937-956. https://doi.org/10.1139/p64-087.
57. Gault W. A. & H. N. Rundle, (1969). Twilight observations of upper atmospheric sodium, potassium, and lithium, *Canadian Journal of Physics*, vol. 47 (1). https://doi.org/10.1139/p69-011.
58. Hunten D. M. & L. Wallace, (1967). Rocket measurements of the sodium dayglow, *Journal of Geophysical Research*, vol. 72(1), pp. 69-79. https://doi.org/10.1029/JZ072i001p00069.
59. Gu Y. Y., J. Qian, G. C. Papen, G. R. Swenson, P. J. Espy, (1995). Concurrent observations of auroral activity and a large sporadic sodium layer event during ANLC-93, *Geophysical Research Letters*, vol. 22(20), pp. 2805-2808. https://doi.org/10.1029/95GL02874
60. Midya, S.K., Sarkar, H. & Manna, A., (2001). Antarctic O3 Depletion - Its Effect on the Variation of Li 6708 Å Emission Line Intensity at McMurdo and Halley Bay. *Czechoslovak Journal of Physics*, vol.51, pp 609–614. https://doi.org/10.1023/A:1017560604799
61. Ghodpage R. N., A. Taori, P. T. Patil, S. Gurubaran. (2013). Simultaneous mesospheric gravity wave measurements in OH night airglow emission from Gadanki and Kolhapur – Indian low latitudes. *Current Science*, vol. 104(1), pp. 98 – 104.
62. Ghodpage R. N., A. Taori, P. T. Patil, S. Gurubaran, A. K. Sharma, S. Nikte, D. Nade, (2014). Airglow Measurements of Gravity Wave Propagation and Damping over Kolhapur (16.8^0N, 74.2^0E), *International Journal of Geophysics*, vol. 2014, pp. 9. https://doi.org/10.1155/2014/514937

63. Shefov, N. N., (1968). 'Intensity and Rotational Temperature Variations of Hydroxyl Emission in the Nightglow', *Nature*, vol. 218, pp. 1238-1239.
64. Shefov, N. N., (1969). 'Hydroxyl Emission of the Upper Atmosphere - I: The Behavior During a Solar Cycle, Seasons and Geomagnetic Disturbances', *Planetary Space Sci*., vol. 17, pp. 797-813.
65. Chamberlain, J. W., (1962). Physics of the aurora and airglow, *Quarterly Journal of the Royal Meteorological Society*, vol. 88 (376), pp. 202.
66. Yee, J.-H., Crowley, G., Roble, R. G., Skinner, W. R., Burrage, M. D., and Hays, P. B., (1997). Global simulations and observations of O (1S), O2 (16) and OH mesospheric nightglow emissions, *Journal of Geophysical Research*, vol. 102(A9), pp. 19949–19968.
67. Baker, D. J., and A. T. Stair Jr. (1988). Rocket measurements of the altitude distributions of the hydroxyl airglow, *Phys. Scr*., vol. 37, pp. 611-622.
68. She, C. Y. and Lowe, R. P., (1998). Seasonal temperature variations in the mesopause region at mid-latitude: comparison of lidar and hydroxyl rotational temperatures using WINDII/UARS OH height profiles, *J. Atmos. Solar Terr. Phys*., vol. 60(16), pp. 1573–1583.
69. Oberheide, J., Offermann, D., Russell III, J. M., and Mlynczak, M. G., (2006). Intercomparison of kinetic temperature from 15μm CO_2 limb emissions and OH*(3, 1) rotational temperature in nearly coincident air masses: SABER, GRIPS, *Geophys. Res. Lett.*, vol. 33(L1), p. 4811, doi:10.1029/2006GL026439.
70. Walter A. Lyons and Michey D. Schmidt (2003). P1.39 The Discovery of Red Sprites as an Opportunity for Informal Science Education. American Meteorological Society. Retrieved on 2009-02-18.
71. Nielsen Stenbaek, H.C., Kanmae, T., McHarg, M.G. et al., (2013). High-Speed Observations of Sprite Streamers. *Surv Geophysics*, vol. 34, pp. 769–795. https://doi.org/10.1007/s10712-013-9224-4.
72. Jehl, A., T. Farges, and E. Blanc (2013). Color pictures of sprites from nondedicated observation on board the International Space Station, *Journal of Geophysical Research-Space Physics*, vol. 118, pp. 454–461. doi:10.1029/2012JA018144.

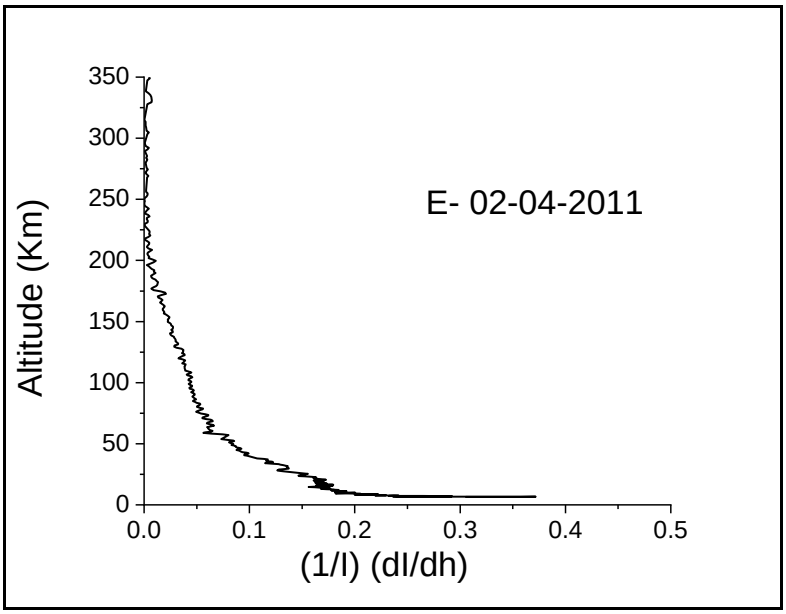

Figure-1: Aerosol vertical profile free from twilight airglow activities

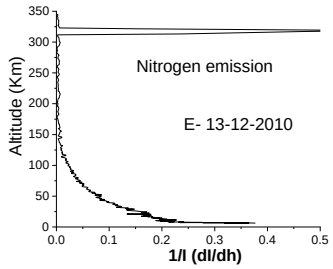

Altitude of Peak: 318.75 km;
Thickness: 11.1 km

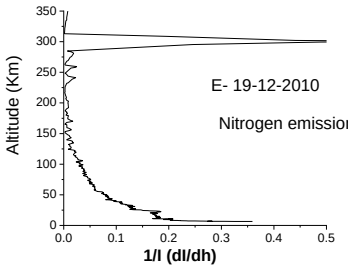

Altitude of Peak: 300.7 km;
Thickness: 28.11 km

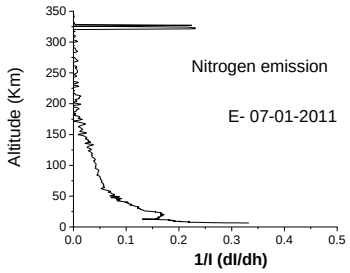

Altitude of Peak: 323.07 km; Thickness: 5.65 km
Altitude of Peak: 327.32 km; Thickness: 2.84 km

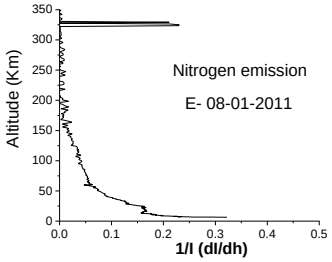

Altitude of Peak: 325.02 km; Thickness: 5.67 km
Altitude of Peak: 329.29 km; Thickness: 2.85 km

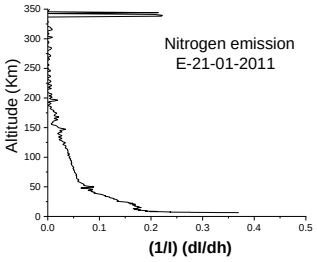

Altitude of Peak: 339.71 km; Thickness: 5.89 km
Altitude of Peak: 344.14 km; Thickness: 2.97 km

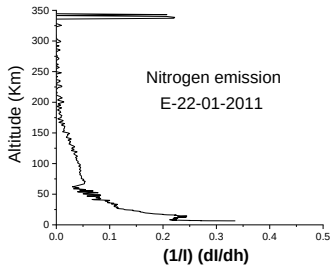

Altitude of Peak: 338.64 km; Thickness: 5.89 km
Altitude of Peak: 343.08 km; Thickness: 2.97 km

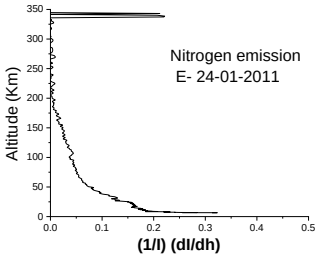

Altitude of Peak: 338.75 km; Thickness: 5.9 km
Altitude of Peak: 343.2 km; Thickness: 2.98 km

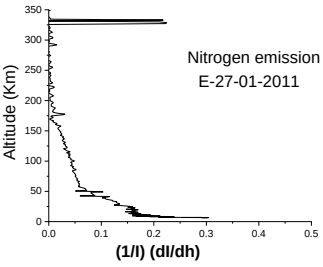

Altitude of Peak: 328.67 km; Thickness: 5.83 km
Altitude of Peak: 333.05 km; Thickness: 2.93 km

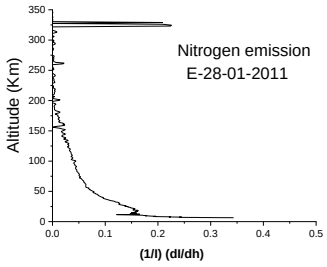

Altitude of Peak: 324.63 km; Thickness: 5.79 km
Altitude of Peak: 328.99 km; Thickness: 2.92 km

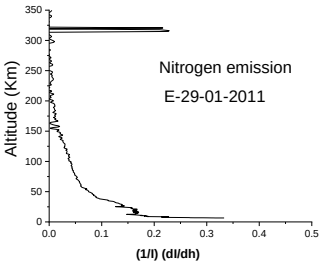

Altitude of Peak: 316.24 km; Thickness: 5.71 km
Altitude of Peak: 320.54 km; Thickness: 2.87 km

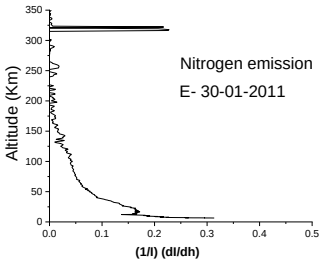

Altitude of Peak: 317.83 km; Thickness: 5.73 km
Altitude of Peak: 322.15 km; Thickness: 2.89 km

717 Figure-2: Twilight airglow emission of ionized nitrogen (N_2)

718

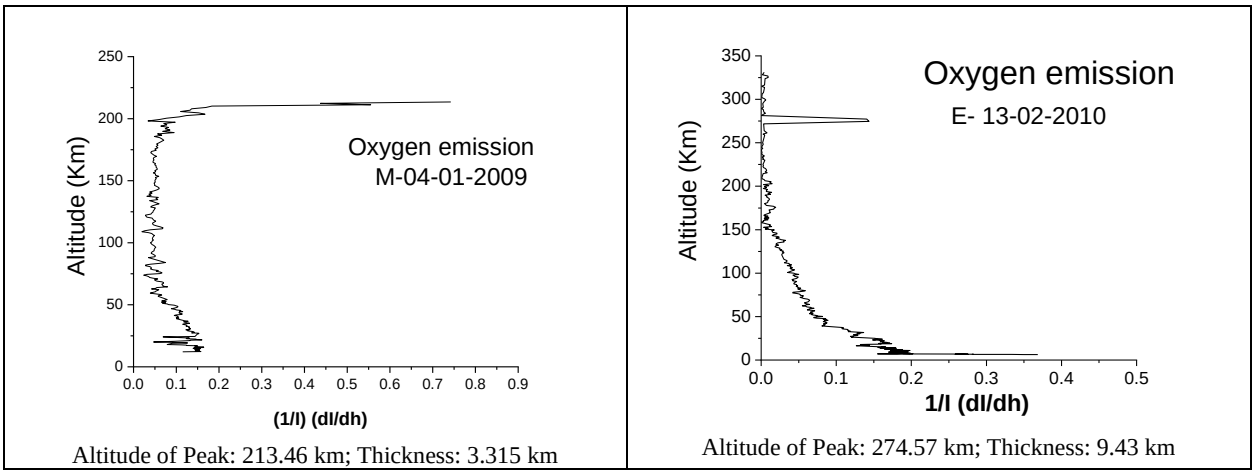

Figure-3: Twilight airglow emissions due to excited oxygen atoms

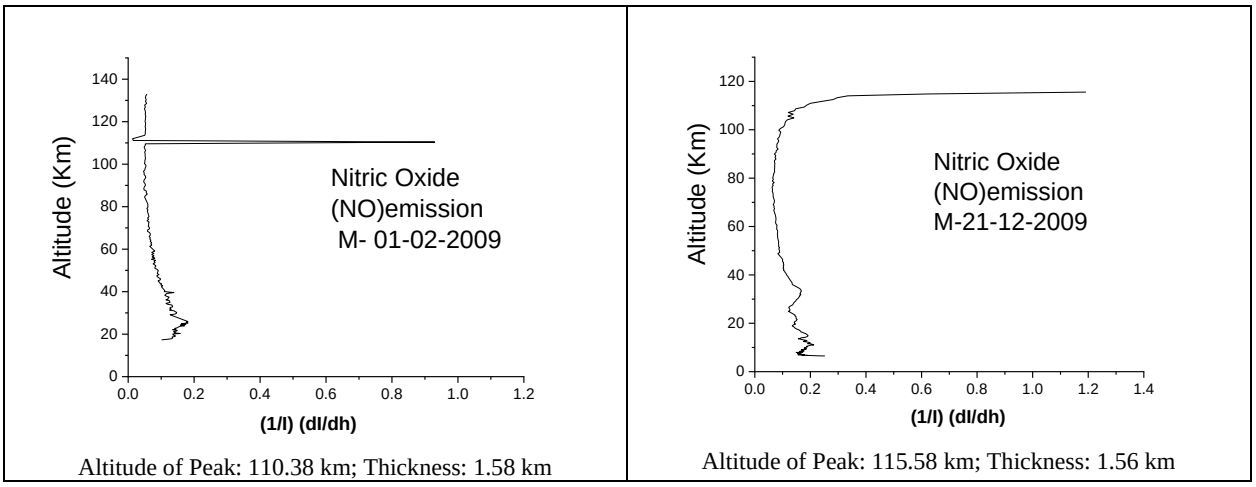

Figure-4: Twilight airglow emission caused by formation of a molecule of nitric oxide (NO)

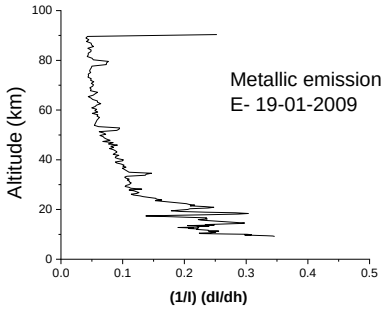

Altitude of Peak: 90.34 km; Thickness: 1.4 km

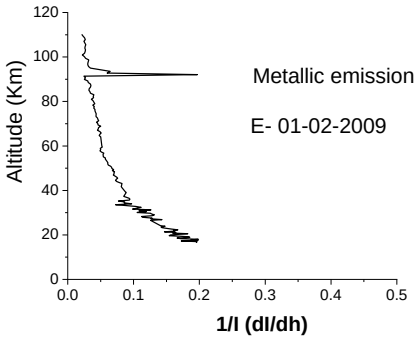

Altitude of Peak: 92.08 km; Thickness: 3.61 km

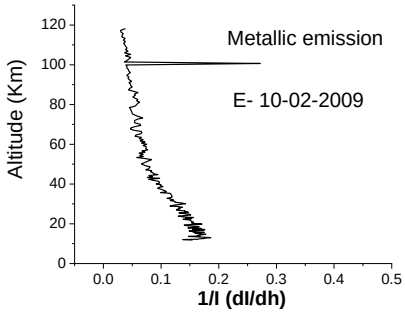

Altitude of Peak: 100.62 km; Thickness: 1.52 km

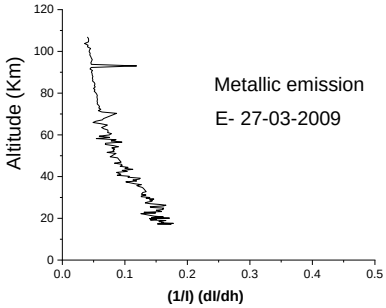

Altitude of Peak: 93.4 km; Thickness: 1.49 km

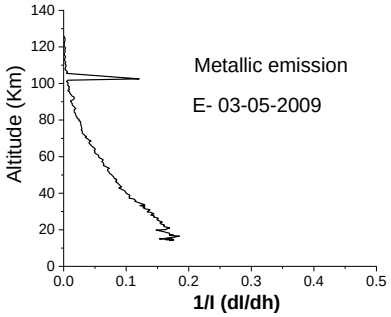

Altitude of Peak: 102.53 km; Thickness: 4.45 km

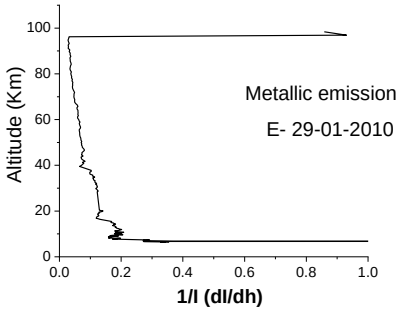

Altitude of Peak: 96.93 km; Thickness: 1.48 km

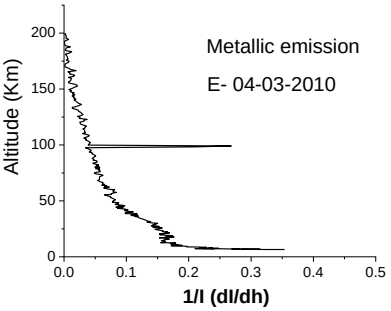

Altitude of Peak: 99.14 km; Thickness: 2.31 km

727 Figure-5: Twilight airglow metallic emissions of sodium and lithium

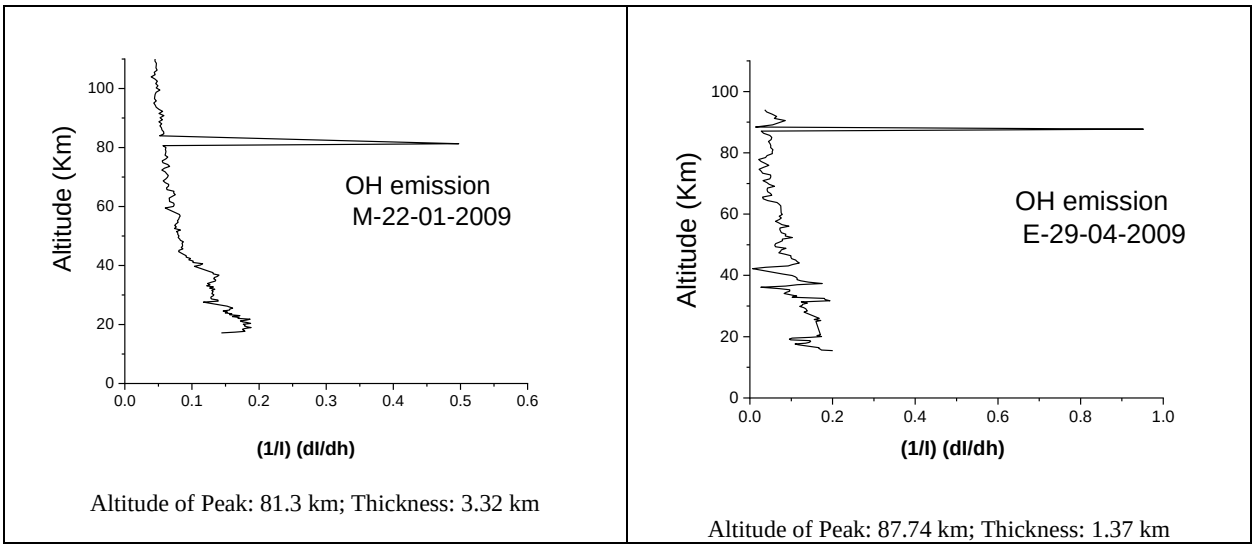

728 Figure-6: OH, twilight airglow layer

729

730

731

732

733

734

735

736

737

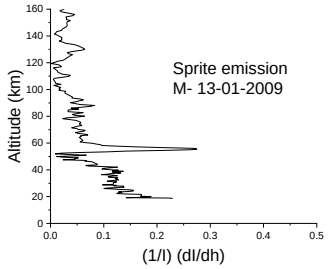

Altitude of Peak: 55.53 km; Thickness: 4.1 km

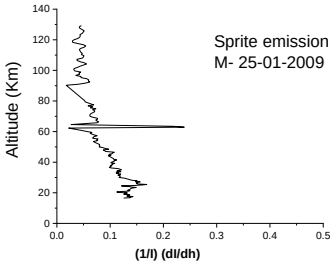

Altitude of Peak: 62.87 km; Thickness: 2.3 km

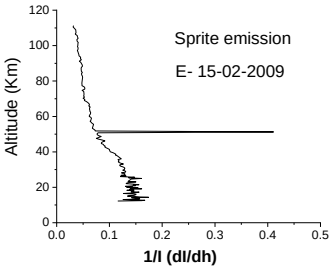

Altitude of Peak: 51.26 km; Thickness: 2.19 km

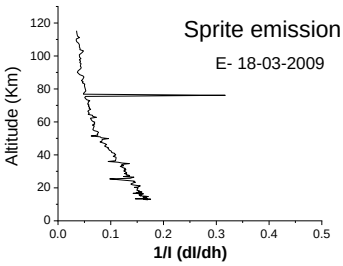

Altitude of Peak: 76.11 km; Thickness: 1.34 km

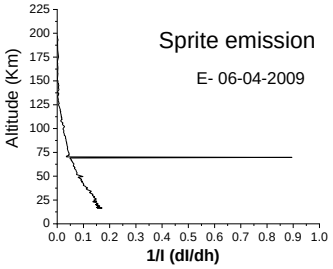

Altitude of Peak: 69.68 km; Thickness: 1.25 km

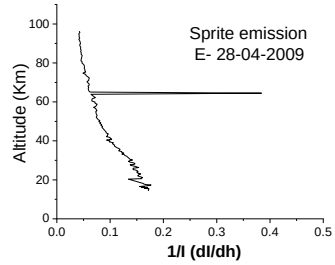

Altitude of Peak: 64.47 km; Thickness: 1.16 km

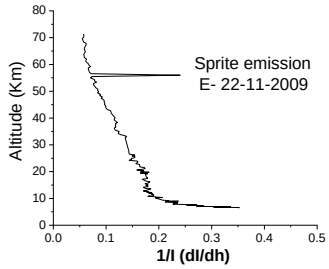

Altitude of Peak: 56.01 km; Thickness: 1.07 km

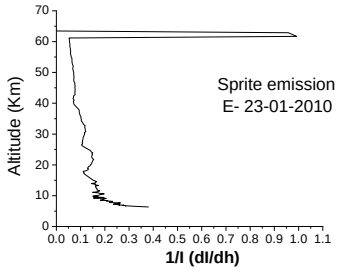

Altitude of Peak: 61.73 km; Thickness: 2.27 km

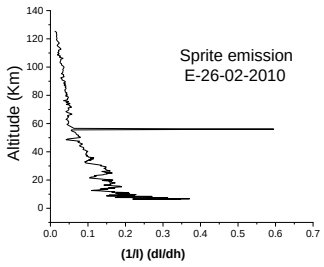

Altitude of Peak: 56.06 km; Thickness: 1.12 km

738 Figure-7: Emission of red sprites during twilight

739

740

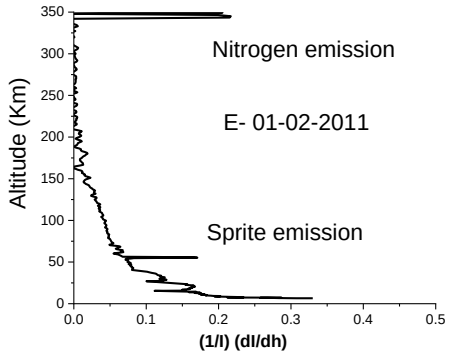

Sprite emission: - Altitude of Peak: 55.25 km; Thickness: 1.62 km

Nitrogen emission: - Altitude of Peak: 345.01 km; Thickness: 6.02 km

Altitude of Peak: 349.54 km; Thickness: 3.04 km

741 Figure-8: Two-layered Twilight airglow red emissions

742

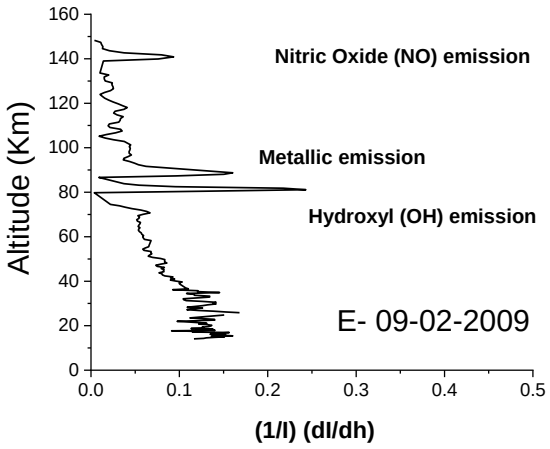

Hydroxyl (OH) emission: - Altitude of Peak: 81.13 km; Thickness: 6.86 km

Metallic emission: - Altitude of Peak: 88.75 km; Thickness: 7.17 km

Nitric Oxide (NO) emission: - Altitude of Peak: 140.84 km; Thickness: 5.53 km

743 Figure-9: Three-layered Twilight airglow red emissions

744